Analysis of Ionospheric Range Delay Corrections for Navigation in South American Low-Latitude Regions

Amalia M. Meza and Laura I. Fernández
Facultad de Cs. Astronómicas y Geofísicas, Universidad de La Plata, Buenos Aires, Argentina
Consejo Nacional de Investigaciones Científicas y Técnicas, CONICET, Argentina

Abstract

Ionospheric conditions for South American low- and mid-latitude scenarios are simulated. The performance of an ionospheric correction algorithm on positioning is analysed for this region. This correction is of similar nature to the Satellite Based Augmentation System (SBAS) type algorithm. The mismodelling produced by each ionospheric simulated approximation can be separately quantified: 1) the single layer shell representation of the ionosphere and 2) the simple geometric mapping function. The effects of both components on positioning are evaluated and discussed for periods with different levels of ionospheric activity: winter, summer, and austral spring equinox. The results show that the mapping function is the most important contributor to the ionospheric error. Its effect on the height component is the most important. Besides, on north and east components, the principal error contributor is the Vertical Total Electron Content (VTEC) mismodelling. The application was also tested on real data during a spring equinox of a mid-low solar activity year (2005) and the results are similar and coherent with those obtained using simulated data.

Keywords: Ionospheric model, TEC, Positioning

1. Introduction

Previous studies on the ionospheric behavior over South American regions have been performed by applying different methods. Ezquer et al. (1998) determined the Total Electron Content (TEC) by using geosynchronous satellite signals, Foppiano et al. (1999) computed the F0F2 and hmF2 from ionograms; and Komjathy et al. (2003) and Fredizzi et al., (2001) calculated TEC from Global Positioning System (GPS) observables.

The GPS consists of a constellation of 32 radio navigation satellites and a ground control subsystem. The satellites broadcast two carrier signals at 1.5754 GHz and 1.2276 GHz, named L1 and L2 respectively, modulated by the so-called P and C/A codes (Seeber, 1993). The GPS-based methods for precisely determining ionospheric TEC/delay are given and summarized in Wu et al. (2006) and Yuan et al. (2007).

The goal of the Satellite Based Augmentation Systems (SBAS) is the validation of the integrity of Global Navigation Satellite System (GNSS) signals, making possible their use in critical services such as civil aviation. A typical SBAS supplies two different sets of corrections. The first set deals with some GPS parameters and it is user position independent. The second set refers to the ionospheric corrections and it is area specific. Generally, typical SBAS structure supplies correction parameters for a number of points organized in a $5° \times 5°$ grid pattern across its service area. The user receiver computes ionospheric corrections for the received GPS signals based on algorithms which use the appropriate grid points where the user is located (Singh, 2005).

Although this work does not constitute any SBAS test bed, the results here obtained can be use as an approximation for the eventual application of an SBAS scheme in South America.

From the perspective of ionospheric activity, the world can be divided into three regions: mid latitudes, the polar caps, and the equatorial region including the equatorial anomaly.

The equatorial region extends up to $\pm$ 30 deg. of geomagnetic latitude. In the equatorial ionosphere the spatial and temporal variability is much greater than in the mid-latitude regions even during quite magnetic conditions (Hargreaves, 1992).

This can mean, for example, that the ionospheric corrections suitable for mid-latitude regions of the northern hemisphere do not produce positions of equal quality in low latitudes of South America.

Meza and Fernández : Analysis of Ionospheric Range Delay Corrections for Navigation in South American Low-Latitude Regions

165

The aim of this work is to detach in components the errors of a numerical simulation of the ionospheric contribution. The last must be applied to the corrections of the coordinates for a GPS station, such as the transmitted ones for an SBAS scheme.

For numerical simulation the ionospheric model NeQuick is used for computing the slant ionospheric range delays. Although this model (like any other theoretical ionospheric model) does not represent a real ionosphere (Aragon-Angel et al., 2005, 2006; Belabbas at al., 2005), the average behaviour of the ionospheric effect is well represented by NeQuick.

Thus, a theoretical ionospheric model is employed for estimating the average ionospheric effect on positioning (north, east, and height), allowing us to monitor the mean ionosphere performance under different scenarios.

To characterize the typical behaviour of the ionosphere, this simulation includes different epochs of solar activity as well as different epochs of the year (spring equinox in the southern hemisphere and solstices). In order to compare and to validate results, the study was performed for South America, focusing on low- and mid-latitude geomagnetic regions.

The work will be presented in three main parts: firstly, the numerical simulation scheme used to assess the accuracy of a GPS-based regional ionospheric model (LPIM) is described; then, an example using real GPS data is provided. Finally we discuss and analyse the effects of LPIM errors on positioning, discriminating between mapping function and model error contribution to the total ionospheric correction.

2. Methodology

2.1 TEC from GPS data
Ionospheric observables from GPS signals will be used in this work, in particular, the so-called geometry free linear combination (ϕ_4)

$$\phi_4 = \phi_1 - \phi_2 = \alpha \cdot STEC + c \cdot (\tau_r + \tau^s) + C_r^s + \upsilon . \quad (1)$$

where ϕ_1 and ϕ_2 are the carrier phase GPS observations at the frequencies L1 and L2; α is a constant; STEC is the Slant Total Electron Content; τ_r and τ^s are inter-frequencies electronic delays produced in the hardware of the receiver and the satellite respectively; c is the speed of light in vacuum; C_r^s is the combination of both carrier phase ambiguities; and υ is the (L1–L2) combined measurement error. STEC can be expressed as the integral of the electron density distribution (N_e) along the signal path from the satellite to the receiver.

For this work we will use the GPS regional ionospheric model La Plata Ionospheric Model (LPIM) (Brunini et al., 2002). LPIM has a good agreement with other Vertical Total Electron Content (VTEC) observable as TOPEX-Poseidon data and with other GPS models (Meza et al., 2002a, 2002b; Brunini et al, 2004, 2005).

The adopted model assumes that the ionosphere is concentrated in a spherical shell of infinitesimal thickness, located at 450 km above the Earth's surface. Within this approximation, the STEC along the signal path is converted into VTEC at the point where the signal pierces the shell, using the approximate mapping function

$$M(z')^{-1} = \frac{VTEC}{STEC}$$
$$= \cos z' \quad (2)$$

where z' is the zenith distance of the signal at the piercing point.

The ambiguities term (C_r^s) is estimated and reduced from Eq. (1) using the less precise but unambiguous P-code phase observations. For regional purposes, the spatial and temporal variability of the VTEC on the shell is represented by a polynomial expansion dependent on the geographic longitude (λ_{pp}) and latitude (φ_{pp}) of the signal piercing point, and the universal time, t, of the observation (Meza et al., 2005b).

2.2 Numerical simulation
The numerical simulation scheme applied in this work is based on Meza et al. (2005a). Briefly, we will describe it below.

The NeQuick model (Hochegger et al., 2000; Radicella and Leitinger, 2001) was used to simulate the geometry free observable (Eq. 1) from the hypothetical network of GPS receivers shown in Fig. 1. NeQuick computes the ionospheric electron density as a function of solar activity, month, Universal Time (UT), height, and geographic coordinates.

The simulated electron density function from the NeQuick model (N_{eNQ}) is used to compute the geometry free linear combination ϕ_4,

$$\phi_{4NQ} = \alpha \cdot \int_{path_r^s} N_{eNQ} \, dl . \quad (3)$$

From Eq. (3), a dataset of geometry free observations with 30-sec sampling rate was simulated for the observing GPS network shown in Fig. 1. The satellite positions were computed from the GPS ephemeris. It should be noted that all the biases and random noise of Eq. (1) were assumed equal to zero in the simulated observations.
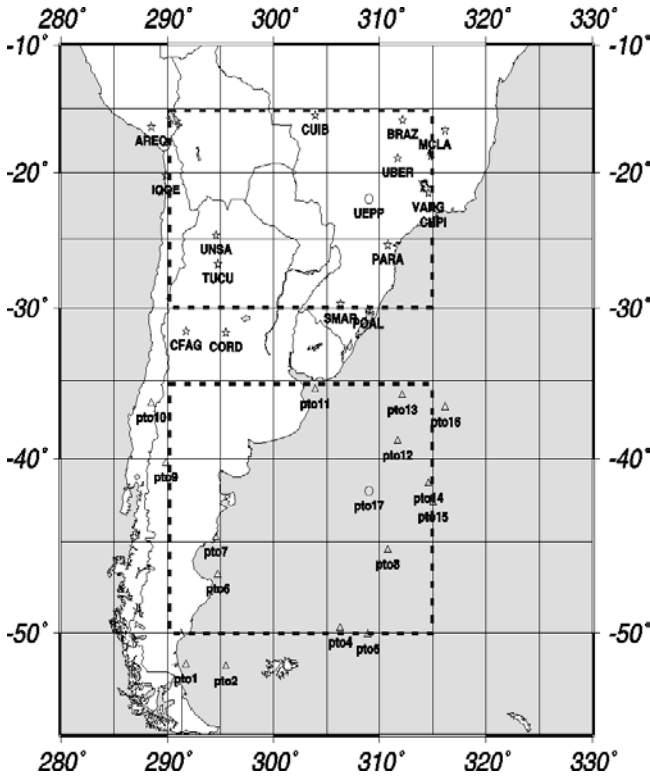
Meza and Fernández : Analysis of Ionospheric Range Delay Corrections for Navigation in South American Low-Latitude Regions

166

Figure 1. Distribution of the receivers for the tracking (☆) and the simulated (Δ) GPS networks. Virtual user's positions are marked by circles (o).
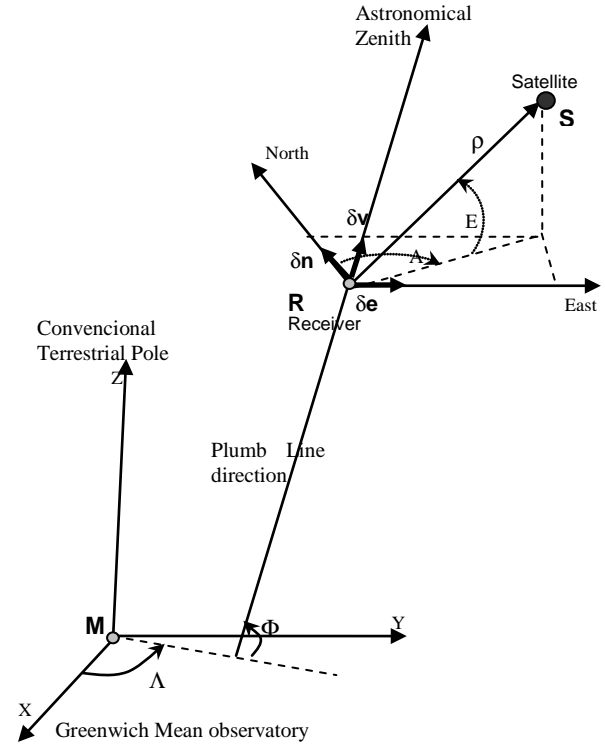

Figure 2: Positioning from satellite observation in the local astronomical system (east, north, zenith) and its link with the Conventional Terrestrial Reference System (X,Y,Z) where the plumb line direction is given by the astronomical latitude (Φ) and longitude (Λ).

Using this simulated dataset, the expansion coefficients and the inter-frequency electronic delays of the VTEC expansion (Meza et al., 2005b) are adjusted by least squares. Then,

$$\phi_{4NQ} = \frac{\alpha}{\cos z'} \, VT\tilde{E}C + c \cdot (\tilde{\tau}_r + \tilde{\tau}^s) + \tilde{\upsilon} . \qquad (4)$$

For the above simulation scheme it is important to note that the inter-frequency electronic delays $(\tilde{\tau}_r, \tilde{\tau}^s)$ and the random noise $\tilde{\upsilon}$ were assumed equal to zero. The estimation of the non-zero values (Eq. 4) is useful to account for any inconsistency between the LPIM and the NeQuick model.

2.3 Effect of the total ionospheric range delay correction on positioning.

In order to understand how the ionospheric range delay error applies to the coordinates, we will start with the fundamental observation equation for GNSS single-point, single-epoch positioning (e.g. Seeber, 1993)

$$\hat{\rho} - \rho_0 = (\cos E \cdot \cos A) \cdot \delta n + (\cos E \cdot \sin A) \cdot \delta e$$
$$+ (\sin E) \cdot \delta v + c \cdot \delta t + \varepsilon \qquad (5)$$

where $\hat{\rho}$ is the observed pseudo-range corrected by the ionospheric and tropospheric delays, relativistic effects, and the satellite clock errors; ρ_0 is the satellite-receiver geometrical range, computed from the a priori receiver coordinates and satellites ephemeris precisely; E and A are the satellite elevation and azimuth, where the elevation angle being the complement of the zenithal distance (z) of the satellite and $(\cos E \cdot \cos A)$, $(\cos E \cdot \sin A)$, $(\sin E)$ are the corresponding direction cosines of the receiver-to-satellite direction (R to S, see Figure 2) with respect to the North-East-Vertical local coordinate system also called the astronomical local horizontal system (Figure 2); c is the speed of light in a vacuum; δn, δe, and δv are the corrections to the a priori receiver coordinates in the local system, δt is the receiver clock error; and ε represents the observation random error. If n satellites are simultaneously observed, the observation equations (5) can be arranged in a linear equation system

$$\Delta\rho = \mathbf{A} \cdot \Delta\mathbf{x} + \varepsilon , \qquad (6)$$

where $\Delta\rho$ is an n × 1 matrix containing the observed minus computed ranges; $\Delta\mathbf{x}$ is a 4 × 1 matrix containing the positioning and time unknowns (δn, δe, δv, δt); ε is an n × 1 matrix containing the observation random

Meza and Fernández : Analysis of Ionospheric Range Delay Corrections for Navigation in South American Low-Latitude Regions

167

errors; and $\mathbf{A}$ is an n × 4 matrix containing the direction cosines and the time unknown coefficient.

Provided that four or more satellites are simultaneously observed (i.e. n ≥ 4), the linear equation system Eq. (6) can be solved by least squares

$$\Delta\mathbf{x} = (\mathbf{A}^t \cdot \mathbf{A})^{-1} \cdot \mathbf{A}^t \cdot \Delta \tag{7}$$

Eq. (7) mathematically expresses the link between the unmodelled errors and their effects on positioning. If the a priori receiver coordinates were perfectly known, the receiver clock were in perfect synchrony with the GPS time, and all the systematic errors affecting the observations were perfectly corrected, the first term of Eq. (6) should be null and thus $\Delta\boldsymbol{\rho} = \mathbf{0}$. Replacing in Eq. (7) will lead to a solution $\Delta\mathbf{x} = \mathbf{0}$, except for the observation random errors. In this work, we will consider that $\Delta\boldsymbol{\rho}$ is affected only by the ionospheric range delay error, that is,

$$\Delta\boldsymbol{\rho} = \alpha\, STEC \tag{8}$$

More specifically, in order to evaluate and analyse the different sources that contribute to the ionospheric error in positioning, we will split the total ionospheric range delay error ($\Delta\boldsymbol{\rho}$), henceforth named as total error, into its components: the error caused by a mismodelling of the total electron content quantity (ΔVTEC) and the error caused by an inadequate election of the mapping function (ΔM(z')).

Moreover, we assume that STEC can be expressed as

$$STEC = STEC_0 + \Delta STEC \tag{9}$$

where $STEC_0$ is a first approach value computed as the integral of the electron density distribution (in this work the NeQuick model is used to represent the electron density) along the signal path. The total error term $\Delta STEC$ can be divided into two terms accounting for a contribution of the error in mapping function (E Δ M) and the error in the VTEC determination (E Δ VTEC), respectively.

Thus, from Eq. (8) and Eq. (9),

$$\Delta\boldsymbol{\rho} = \alpha\, (STEC_0 + \Delta STEC) \tag{10}$$

Any other components affecting the error of total ionospheric range correction are neglected as asseverated in the previous work of Meza et al., (2005a). With respect to the GPS clock delay, although it takes an important part of the total ionospheric range delay correction, it does not have an important influence on positioning.

Therefore,

$$\Delta STEC = \left.\frac{\partial \Delta STEC}{\partial M}\right]_0 \Delta M + \left.\frac{\partial \Delta STEC}{\partial VTEC}\right]_0 \Delta VTEC \tag{11}$$

where the variations in the mapping function and the model used to estimate the VTEC values can be expressed as

$$\Delta M = M_{LPIM} - \frac{STEC_0}{VTEC_0} \tag{12}$$

$$\Delta VTEC = VTEC_{LPIM} - VTEC_0$$

where M_{LPIM} is the mapping function at the user position from the LPIM model (z' is the zenith distance of the signal at the piercing point), $VTEC_{LPIM}$ refers to the vertical total electron content computed by the LPIM model, and the $VTEC_0$ is the vertical total electron content computed as the integral of the electron density distribution (using the theoretical model as NeQuick) in the vertical direction at the piercing point.

From Eqs (10), (11), and (12),

$$\Delta\rho = \alpha\, STEC_0 + \alpha\, \left.\frac{\partial \Delta STEC}{\partial M}\right]_0 \left[M_{LPIM} - \frac{STEC_0}{VTEC_0} \right] + \alpha\, \left.\frac{\partial \Delta STEC}{\partial VTEC}\right]_0 [VTEC_{LPIM} - VTEC_0] \tag{13}$$

Then, the contribution of the error in the mapping function and the error in the VTEC estimation to the total ionospheric range delay error can be written as

$$E\Delta M = VTEC_0 \left(M_{LPIM} - \frac{STEC_0}{VTEC_0} \right) \tag{14}$$

$$E\Delta VTEC = M_0 \left(VTEC_{LPIM} - VTEC_0 \right)$$

Therefore, Eq. (13) becomes

$$\Delta\rho = \alpha \left[STEC_0 + E\Delta M + E\Delta VTEC \right] \tag{15}$$

Equation (14) is the key of this work. We will use it to analyse and compare the effects of ionospheric error on coordinates and clock estimates but discriminating by error source.

2.4 Description of the chosen scenery

The areas chosen for this study are two regions in South America. The first is located at low geomagnetic latitudes (ϕ_g), between 290° and 315° longitude and between –15° and –30° latitude. The second one is at mid latitudes, located between 290° and 315° longitude and between –35° and –50° latitude (Fig. 1).

Meza and Fernández : Analysis of Ionospheric Range Delay Corrections for Navigation in South American Low-Latitude Regions

168

From the ionospheric point of view, these areas show different behaviours. In the first one the Equatorial Anomaly has a strong influence, so a great ionospheric variability is expected, depending on the azimuth and elevation of the observed satellites. In the second one the ionosphere shows quiet behaviour, with a smooth variation with latitudes.

Sixteen GPS receivers marked with asterisks in Fig. 1 compose the tracking network (these stations belong to IGS network, http://igscb.jpl.nasa.gov/), and another sixteen GPS receivers marked with triangles in Fig. 1 compose the simulated-tracking network.

At this step it is important to note that several points of the simulated tracking network are located over the ocean. This point would be a serious operational hindrance if trying to perform a test bed of any augmentation system for the region. Nevertheless, our objective is just to simulate the behaviour of the ionosphere over this particular region of the southern hemisphere and thus to estimate an order of magnitude for the probable errors affecting positioning.

We also consider a user in each sector marked with a circle in Fig. 1, located in the central part of the region covered by the tracking stations. The study was undertaken for the years 1996 and 2000, which correspond to periods near minimum and maximum solar activity respectively. During the summer, equinox, and winter, the ionosphere presents different behaviour. These three epochs of the years 1996 and 2000 were chosen to carry out the analysis. Due to the fact that NeQuick can reproduce not the small day by day variability but instead a smooth ionospheric behaviour, selecting one day per season is enough to fulfil the task.

In order to evaluate the discrepancies between the ionospheric range delay and the respective LPIM corrections, we proceeded as follows:

1) Using the methodology explained in Section 2.2, a time-dependent Grid Ionospheric Vertical Delay (GIVD) was computed at each Ionospheric Grid Point (IGP) of a $5° \times 5°$ grid covering the hypothetical SBAS region (Fig. 1), where the path considered (Eq. 3) is the vertical one at each grid point.

2) The User Ionospheric Vertical Delays (UIVD), from the virtual observer located at the GPS station UEPP (Presidente Prudente $–22.1°$ S; $51.4°$ W, Brazil), were obtained by interpolation from the nearby GIVD.

3) The UIVD were converted into slant ionospheric range delay using the mapping function (Eq. 2).

4) The UIVD effect in positioning was computed by solving the positioning problem discussed in Section 2.3, where $\Delta\mathbf{x}$ can be written as

$$\Delta\mathbf{x} = (\mathbf{A}^t \cdot \mathbf{A})^{-1} \cdot \mathbf{A}^t \cdot \alpha \, \text{STEC}$$
$$= (\mathbf{A}^t \cdot \mathbf{A})^{-1} \cdot \mathbf{A}^t \cdot \alpha \, \frac{\text{UIVD}}{M(z')} \qquad (16)$$

5) The NeQuick slant ionospheric range delay effect in positioning was computed by solving the problem discussed in Section 2.3, Eq. (7). We assumed this range delay effect to be the "true ionospheric correction" in a scene of simulation or "ionospheric correction of reference". Consequently "true" does not mean a real representation. Therefore, we called the four-vector of time and positioning variations $\Delta\mathbf{x}_0$ the "true ionospheric correction" where

$$\Delta\mathbf{x}_0 = (\mathbf{A}^t \cdot \mathbf{A})^{-1} \cdot \mathbf{A}^t \cdot \alpha \, \text{STEC}_0 \qquad (17)$$

where STEC_0 is estimated from NeQuick.

Finally, we define as the error of the ionospheric corrections in positioning the difference between $\Delta\mathbf{x}_0$ and $\Delta\mathbf{x}$:

$$\Delta\varepsilon_i = \Delta\mathbf{x}_0 - \Delta\mathbf{x}$$
$$= \left[(\mathbf{A}^t \cdot \mathbf{A})^{-1} \cdot \mathbf{A}^t \right] \cdot (\text{STEC}_0 - \text{STEC}) \qquad (18)$$
$$= \left[(\mathbf{A}^t \cdot \mathbf{A})^{-1} \cdot \mathbf{A}^t \right] \cdot \Delta\text{STEC}$$

From this expression we can analyse the effect produced by the error of the mapping function and the VTEC mismodelling. Effectively, following Eqs. (7) to (15) we replaced $\Delta STEC$ in Eq. (18) with the expression

$$\Delta\text{STEC} = \text{E}\Delta\text{M} + \text{E}\Delta\text{VTEC} \qquad (19)$$

where $\text{E}\Delta\text{M}$ is the mapping function error assuming there is no error in the VTEC representation and $\text{E}\Delta\text{VTEC}$ is the error in the VTEC determination if we suppose that there is no error in mapping function.

3. Results

3.1 The simulated GPS data
The methodology described in Section 2.2 was applied to the scenery shown in Figure 1 and described in Section 2.4 for the southern hemisphere. The region was divided into two sub-regions: one for the low geomagnetic latitudes ($–35° \leq \phi_g \leq –15°$) and one for the mid-geomagnetic latitudes ($–50° \leq \phi_g \leq –35°$). The ionospheric behaviour in the area was simulated for two periods (including two solstices and austral spring

Meza and Fernández : Analysis of Ionospheric Range Delay Corrections for Navigation in South American Low-Latitude Regions
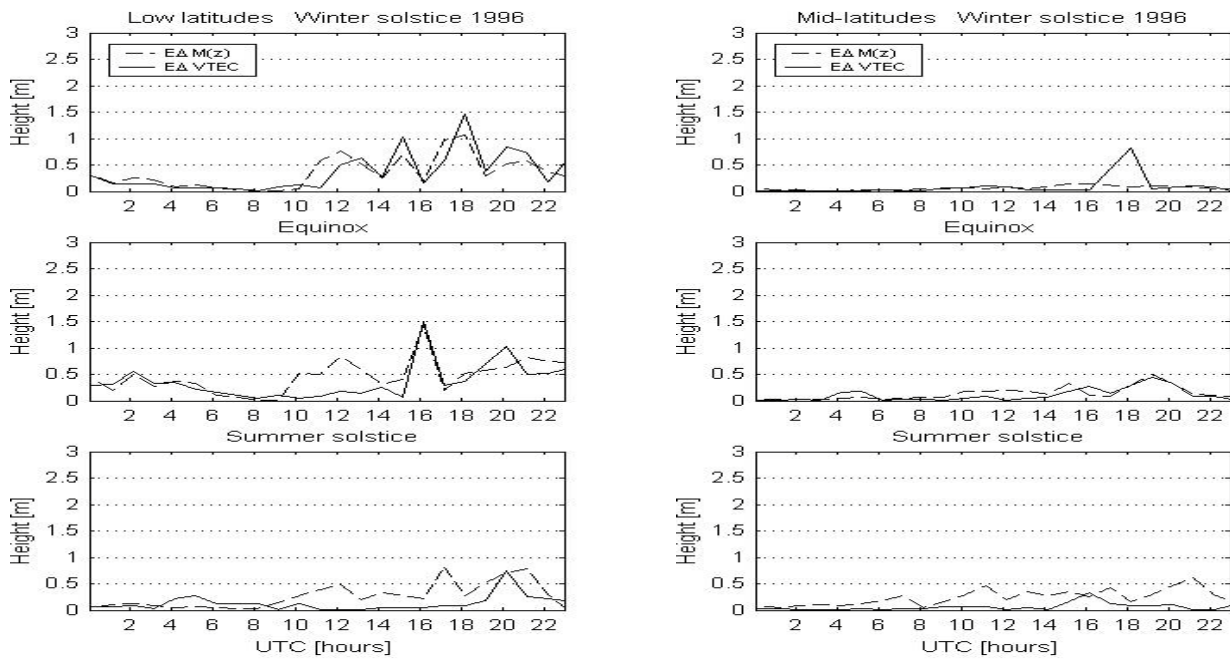
169

Figure 3: Variation in the mapping function (dotted) and VTEC (solid) error for the height component as a function of the Universal Coordinate Time UTC during 1996 at low (left) and mid (right) latitudes in the southern hemisphere
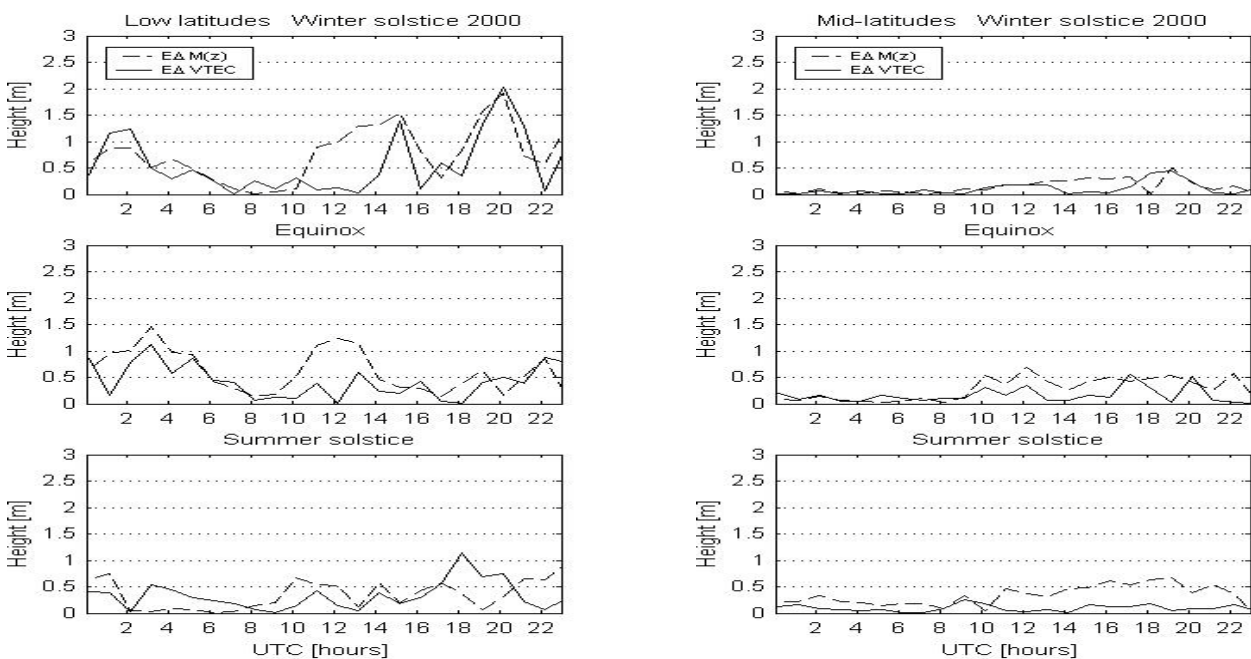

Figure 4 Variation in the mapping function (dotted) and VTEC (solid) error for the height component as a function of the Universal Coordinate Time UTC during 2000 at low (left) and mid (right) latitudes in the southern hemisphere

equinox) of the minimum (1996) and maximum (2000) solar activity, respectively.

From Figures 3 and 4 we can clearly see the expected different ionospheric behaviours at the same latitudes depending on the minimum (1996) or maximum (2000) solar activity. Effectively, the magnitude of the ionospheric error reaches 2 metres in 2000, while in 1996 it never exceeds the 1.5 metre value. Moreover, at low geomagnetic latitudes, we can also distinguish bigger quantities of the error in winter and equinox than in summer despite the different solar activity conditions. On

Meza and Fernández : Analysis of Ionospheric Range Delay Corrections for Navigation in South American Low-Latitude Regions

170

the contrary, at mid latitudes the biggest error in mapping function appears during the equinox and summer.

Meza et al. (2005a) simulated an SBAS scheme for a low geomagnetic latitude region on the African territory. They also used an LPIM model for the estimation of the ionospheric correction during low and high solar activity periods. Nevertheless, they never characterize the effects of the relative contributions of the ionospheric mismodelling $(E \Delta VTEC)$ and the choice of an inadequate mapping function $(E \Delta M)$ on the total ionospheric range errors $(\Delta STEC)$. Besides, they do not include mid-latitude regions in their analysis. However, because of some similarities in the procedure followed, the results of Meza et al. (2005a) were compared to the respective computations for the low geomagnetic South American region.
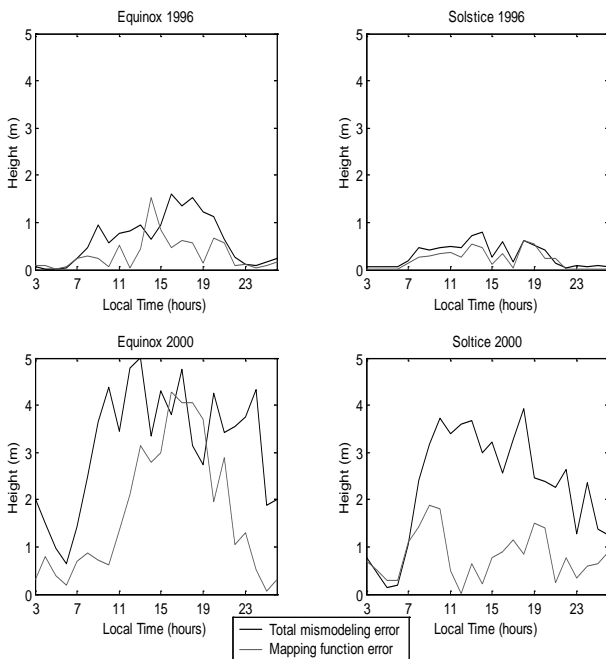
Figure 5: Variation in the ionospheric error for the height component as a function of the Universal Coordinate Time UTC during 1996 and 2000, from Meza et al. (2005a).

When comparing Figures 3 and 4 with Figure 5 from Meza et al. (2005), we can conclude that the behaviours of the errors at low latitudes during low solar activity (1996) are comparable. In contrast, the values of the $\Delta VTEC$ are incremented (by up to 5 metres) during the equinox with the maximum solar activity in Africa with respect to our working scenery in South America. A probably reason for this effect is that the region chosen by Meza et al. (2005a) in Africa is located on the geographic equator whereas the area proposed in this work does not.

Figures 6 and 7 show the r.m.s. in metres computed for the components of the total ionospheric error (north, east,
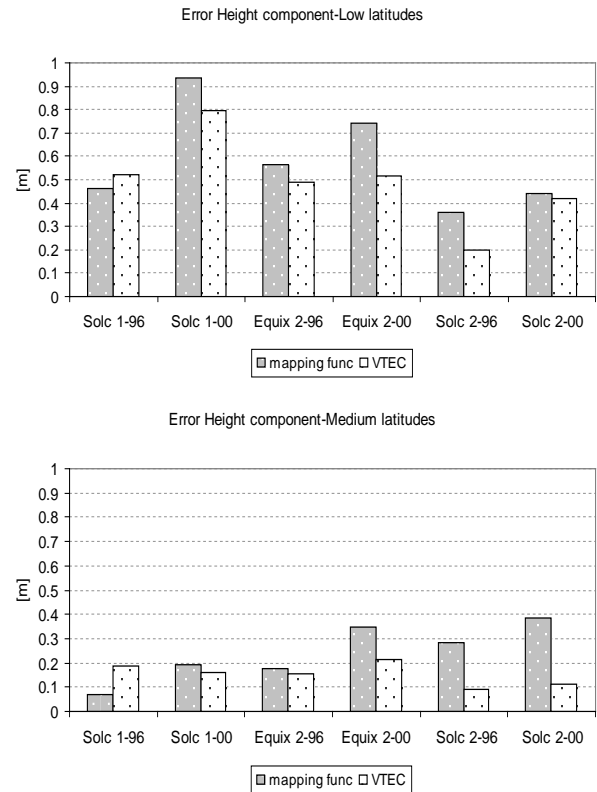
Figure 6: Comparison of the mapping function and VTEC errors with respect to the total ionospheric error for the height component at low- and mid-latitude regions. These plots also compare the magnitude of the errors for different periods of solar activity (in 1996, near a minimum, and in a maximum in 2000), as well as for different epochs of the year, when the ionosphere presents different behaviours.

and height). Values were calculated for the two solstices and the spring equinox of the years 1996 and 2000, respectively.

From Figure 6 we can observe that the ionospheric errors are always more important at low latitudes where they reach values near 0.9 metres, whereas at the mid-latitude regions they only come up to 0.4 metres. This is another expected feature regarding the proximity to the ionospheric equatorial anomaly.

Focusing on the height component at low-latitude regions, Figure 6 (based on Eq. (14) and Eq. (18)) show us that the error produced by the mapping function becomes the most important contributor although the error achieved by an inadequate VTEC model is sometimes scarcely minor. The previous rule is not fulfilled in the winter of 1996.

We have to take into account that the mapping function error should be affected by the presence of horizontal gradients in the electron density distribution. Thus, the error in mapping function estimated $(\Delta M(z))$ in this work represents a level of minimal variation of this effect. Thus we can conclude from Figure 6 that the error of the

Meza and Fernández : Analysis of Ionospheric Range Delay Corrections for Navigation in South American Low-Latitude Regions
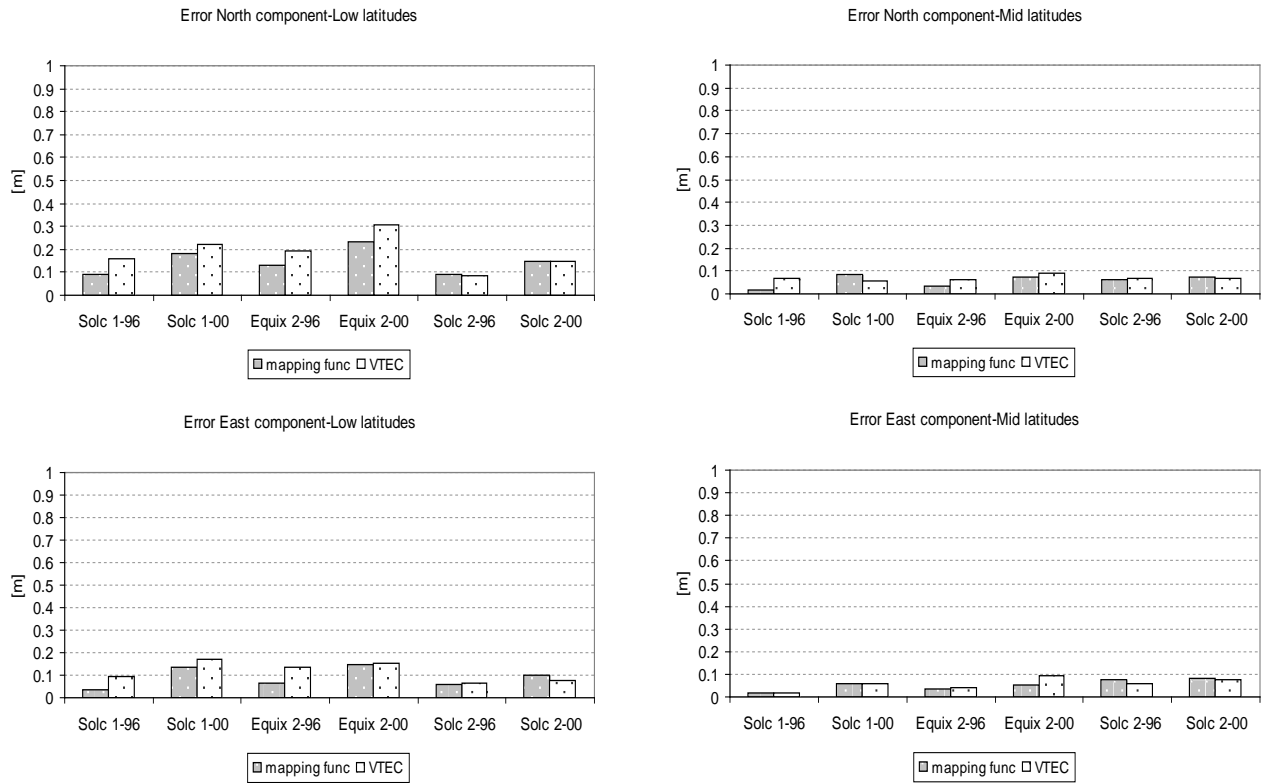
171

Figure 7: Comparison of the mapping function and VTEC errors with respect to the total ionospheric error for the north and east components at low- and mid-latitude regions. These plots also compare the magnitude of the errors for different periods of solar activity (in 1996, near a minimum, and during a maximum in 2000), as well as for different epochs of the year, when the ionosphere presents different behaviours

mapping function is the dominant effect at low and mid latitudes.

Regarding Figure 7 (based on Eq. (14) and Eq. (18)) we note that for both: north and east components, the effect of the VTEC error is the main source contributing to the range error. The total ionospheric error for the northern component can reach almost 0.3 metres (which occurred at low latitude). This value is comparable with the typical values that the height component reaches at mid geomagnetic latitudes. Nevertheless for the east component, even in the worst conditions, at low latitudes and maximum solar activity, the total ionospheric range error is never bigger than 0.2 metres.

3.2 The real GPS data.

The measurements from 16 GPS stations distributed at low latitudes ($-35° \leq \phi_g \leq -15°$) in South America (see Figure 1) were used to carry out the previous analysis but using real data. This region has a great ionospheric variability because it is close to the Equatorial Anomaly. By using real data, it is impossible to divide the error into the two components, as shown in Section 2.3 ($E\Delta M$ and $E\Delta VTEC$). Instead the effect of the total ionospheric

range delay correction on positioning will be represented and analysed.

The measurements used belong to a quiet geomagnetic day: 6 September 2005. Accordingly, the variations in the ionospheric correction can be related with those corrections proposed in the simulation analysis described above.

Thus, using the same procedure specified in the simulation to evaluate the discrepancies between the ionospheric range delay and the respective LPIM corrections, we proceed as follows:

Firstly, we apply the methodology explained in Section 2.4 to compute a time-dependent Grid Ionospheric Vertical Delay (GIVD) at each Ionospheric Grid Point (IGP) of a 5° × 5° grid covering the upper region of Fig. 1.

Then, the GPS receiver UEPP (–22.1° S; 51.4° W; Presidente Prudente, Brasil) was chosen as the virtual observer. Accordingly, its User Ionospheric Vertical Delays (UIVD) were obtained by interpolation from the nearby point in the GIVD. The UIVD were converted into slant ionospheric range delay using the mapping function (Eq. 2).

Meza and Fernández : Analysis of Ionospheric Range Delay Corrections for Navigation in South American Low-Latitude Regions
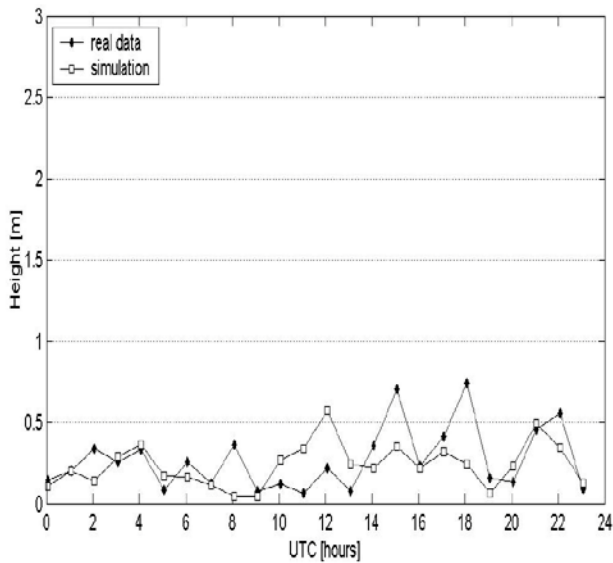
172

Figure 8: Variation in the total ionospheric residual for the height component as a function of the Universal Coordinate Time UTC for the spring equinox in the southern hemisphere during 2005 using real data.

After that, the UIVD effect on positioning was computed by solving the positioning problem discussed in Section 2.4, Eq. 16.

Finally, the "real" slant ionospheric range delays were obtained by using Eq. (1). The STEC effect on positioning was computed by solving Eq. (17) in Section 2.4.

Figure 8 shows the variation in the total ionospheric residual for the height component using real and simulated data. All values are lower than 0.7 m. During night-time hours both variations have similar representations, while for sunrise to sunset both components show differences up to 0.4 m.

4. Conclusions and Suggestions

This work focuses on the analysis of the accuracy of the ionospheric range delay corrections at low and mid latitudes.

The accuracy is evaluated by comparing the ionospheric range delay and its correction. The comparison was performed for the effects of ionospheric error on user coordinates. Thus, it shows the accuracy of the corrections in the position and not in the pseudo-ranges, which do not have a clear meaning for navigation purposes.

With this aim, from simulated data, we computed the effect of ionospheric correction error on the user coordinates considering two components: mapping function error and VTEC mismodelling.

The behaviour of both components of the ionospheric error in the height depends on geographical location and solar activity. Their values are largest at low latitude and high solar activity. Taking into account that the error in mapping function estimated in this work represents a level of minimal variation of this effect, the mapping function is found to be the main contributor to ionospheric error at low latitudes as well as at mid latitudes.

The north and east components of the ionospheric range error are lower than the respective one for the height. Besides, their main contributor is the VTEC mismodelling.

The results using real data are similar and coherent with those obtained using simulated data as shown in Figure 8. During the night the ionospheric error proves to be bounded below 0.5 m for both the real values and the simulated ones. Nevertheless during the day, when the radiative effect of the sun on the ionosphere is evident, the differences between the real values and the simulated ones are increased by a factor of two, showing peaks during the local midday. Despite this, the general agreement of the simulated ionospheric error in positioning with respect to the real computed values is very good. Thus we can speculate that the mapping function error and VTEC mismodelling can be represented by Equation (14).

5. References:

Aragon-Angel M.A., R. Orus, M. Amarillo, M. Hernandez-Pajares, J.M. Juan and J. Sanz (2005), **Preliminary NeQuick assessment for future single frequency users of GALILEO**, In: Proceeding of the 6th Geomatic Week, Barcelona, Spain, February, 8-11.

Aragon-Angel M.A. and F.A. Fernandez (2006), **Advanced ionospheric modeling for GNSS Single Frequency Users**, In: Position, Location, And Navigation Symposium, 2006 IEEE/ION, April 25-27.

Belabbas B., S. Schlueter and M.Z. Sadeque (2005), **Impact of NeQuick correction model to positioning and timing accuracy using the instantaneous pseudorange error of single frequency absolute positioning receivers**, In: Proceedings of ION GNSS 2005, 13-16 September, Long Beach, California: 712-722.

Brunini, C.; M. A. VanZele; A. Meza y M. Gende (2002); **Quiet and perturbed ionospheric representation according the electron content from GPS signals**, Journal of Geophysical Research (Space Physics) Vol. 108 No. A2 10.1029/2002JA009346.

Brunini, C., Van Zele, M.A., Meza, A., Gende, M. (2003) **Quiet and perturbed ionospheric representation according to the electron content from GPS signals**. J. Geophys. Res. 108, DOI 10.1029/2002JA009346.

Brunini C.A., A. Meza, F. Azpilicueta, M.A.Van Zele, M.Gende and A. Díaz; (2004). **A new ionosphere**

Meza and Fernández : Analysis of Ionospheric Range Delay Corrections for Navigation in South American Low-Latitude Regions

173

monitoring technology based on GPS. Astrophysics and Space Science; Kluwer Academic Publishers, Vol. 290, 3-4: 415-429.

Brunini C., A. Meza and W. Bosch (2005); **Temporal and spatial variability of the bias between TOPEX and GPS derived TEC**, Journal of Geodesy, (79), 4-5: 175-188.

Ezquer, R.G., Jadur, C.A., Mosert de Gonzalez, M. (1998) **IRI–95 TEC predictions for the South American peak of the equatorial anomaly**. Adv. Space Res. 22 (6): 811–814.

Fedrizzi, M., Langley, R.B., Komjathy, A., Santos, M.C., de Paula., E.R. Kantor, I.J. (2001) **The low-latitude Ionosphere: Monitoring its behaviour with GPS**. in: Proceedings of ION GPS-2001, Salt lake City, Institute of Navigation: 2468–2475.

Foppiano A.J.1; Cid L.; Jara V. (1999) **Ionospheric long-term trends for South American mid-latitudes** Journal of Atmospheric and Solar-Terrestrial Physics, Volume 61, Number 9: 717-723(7)

Hargreaves, J. K., (1992), **The solar-terrestrial environment**, Cambridge University Press.

Hochegger, G., Nava, B., Radicella, S.M., Leitinger, R. (2000) **A Family of Ionospheric Models for Different Uses**. Phys. Chem. Earth. Vol. 25, 4: 307-310.

Komjathy A., Sparks L., Mannucci A. J. , Pi X. (2003) **An assessment of the current WAAS ionospheric correction algorithm in the South American region**. Journal of the Institute of Navigation, 3, 2003: 193-204

Meza, A., Diaz, A., Brunini, C. and Van Zele, M., (2002a). **Systematic behavior of semiempirical ionospheric models in quiet geomagnetic conditions**. Radio Science, Vol. 3, No. 3: 24-36.

Meza, A., C. A. Brunini, W. Bosch, M.A VanZele (2002b); **Comparing vertical total electron content from GPS, bent and IRI models with TOPEX-POSEIDON**. ASR, (30) 2: 307-312.

Meza A., M. Gende, C. Brunini, S. M. Radicella (2005a) **Evaluating the Accuracy of Ionospheric Range Delay Corrections for Navigation at Low Latitude**, Advances in Space Research, 36: 546-551

Meza, A.; M. A. Van Zele; C. Brunini y R. Cabassi (2005b). **Vertical Total electron content at subauroral and mid-south latitude, during geomagnetic storms**. Journal of Atmospheric and Solar terrestrial Physics, (67), 4: 315-323

Radicella S.M.; Leitinger R. (2001) **Evolution of the DGR approach to model electron density profiles**, Advances in Space Research 27 (1): 35–40,.

Seeber, G. (1993) **Satellite Geodesy**, Walter de Gruyter.

Singh A., (2005) **GAGAN - A visionary approach**. Coordinates Vol. 1, 2: 16-19.

Wu S., Zhang K., Yuan Y. and Wu F. (2006) **Spatio-Temporal characteristics of the ionospheric TEC variation for GPSnet-based real-time positioning in Victoria**. Journal of Global Positioning System, 5 (1-2): 52-57

Yuan Y., Huo X. and Ou J. (2007) **Models and Methods for precise determination of ionospheric delays using GPS.** Progress in Natural Science, 17 (2): 187-196